Effect of thermal history on the deformation of non-metallic inclusions during plain strain compression

Authors:

Dr. Yi Wang
Lecturer at School of Metallurgical and Ecological Engineering, University of Science and Technology Beijing (USTB), Beijing 100083, China
Email: wangyi@metall.ustb.edu.cn

Prof. Lifeng Zhang (Correspondence Author)
Professor at State Key Laboratory of Metastable Materials Science and Technology, School of Mechanical Engineering, Yanshan University, Qinhuangdao City, Hebei Province 066004, China
Email: zhanglifeng@ysu.edu.cn
Phone number: 86-0335-8074666

Prof. Ying Ren (Correspondence Author)
Professor at School of Metallurgical and Ecological Engineering, University of Science and Technology Beijing (USTB), Beijing 100083, China
Email: yingren@ustb.edu.cn

Dr. Zushu Li (Correspondence Author)
Reader at Advanced Steel Research Centre, WMG, University of Warwick, Coventry, CV4 7AL, U.K.
Email: z.li.19@warwick.ac.uk

Dr. Carl Slater
Research fellow at Advanced Steel Research Centre, WMG, University of Warwick, Coventry, CV4 7AL, U.K.
Email: c.d.slater@warwick.ac.uk

Mr. Kaiyu Peng
PhD. student at School of Metallurgical and Ecological Engineering, University of

Science and Technology Beijing (USTB), Beijing 100083, China
Email: pengkaiyu_sgqg@163.com

Mr. Fenggang Liu
PhD. student at School of Metallurgical and Ecological Engineering, University of Science and Technology Beijing (USTB), Beijing 100083, China
Email: liufenggang_sgqg@163.com

Mr. Yanyu Zhao
PhD. student at School of Metallurgical and Ecological Engineering, University of Science and Technology Beijing (USTB), Beijing 100083, China
Email: zhaoyanyu_sgqg@163.com

Abstract: The deformation of inclusions in the steel was affected by the thermal history during the physical simulation of steel processing. After plain strain compression with a reduction of 30%, the average aspect ratio of inclusions in the steel sample cooled down to 1673 K from semi-solid state was 1.89, which was significantly higher than 1.29 in the steel sample heated persistently up to the same temperature. The mechanism was revealed by inclusion transformation.

Keywords: Inclusion deformation, thermal history, inclusion transformation, semi-solid steel

Steel samples were heated up from the cold state to a target temperature during physical simulations, which was usually below 1373 K in Gleeble simulations for hot rolling process[1, 2]. This temperature was designed based on that in the steel production, while the thermal history was quite different, especially in continuous casting-hot charging rolling (CC-HCR) or continuous casting-direct rolling (CC-DR) process. For the steel matrix, studies on physical simulation of continuous casting showed that the hot ductility of steels was affected by the thermal history [3, 4]. The hot ductility of specimen subjected to a thermal history similar to that of billet continuous casting, which included a major temperature drop that occurred just below the mold, a reheat of the surface, and a relatively slow cooling to the unbending temperature, was lower than that predicted by conventional isothermal test. For non-metallic inclusions in pipeline steels, the deformation of alumina with different modification extents and sizes was related to the inclusion composition and the morphology of CaS phase in inclusions[5]. The elongation of precipitates varied with inclusion composition[6, 7]. Moreover, it was found in the study on deformation behaviors of oxide inclusions that the phase transformation occurred during the multi-pass hot rolling process[8]. It was reported that in Al-killed Ca-treated steels, CaO in inclusions was transformed into CaS during continuous casting[9], as well as heat treatment[10]. The deformation behavior of inclusions during the rolling process was related to the transformation ratio of inclusions, which was influenced by the thermal history. Small size calcium aluminate inclusions with low melting temperature were deformed very well along the hot rolling direction regardless of the CaS layer. For inclusions with large size, calcium aluminate oxide inclusions were continuously deformed during hot rolling, while CaS and spinel complex inclusions were divided into several parts[5, 11]. Physical simulation of continuous casting and rolling process can provide an insight into the properties and performances of steel product. However, it was usually performed by heating a cold material to the target temperature instead of undergoing the actual thermal history[12]. Errors caused by the inaccurate thermal history can not be ignored for the consideration of both the steel matrix and inclusions.

The current study was to demonstrate that not only temperature but also the thermal process should be designed based on the simulated process when the deformation of inclusions was concerned. Deformation of inclusions in the semi-solid steel matrix was also investigated.

Steel samples were cut from a slab of a pipeline steel and polished. Main composition of the steel is listed in **Table I**. A Gleeble HDS-V40 thermomechanical simulator was used for direct resistance heating and plain strain deformation trials. Steel samples with the size of 160 mm x 10 mm x 25 mm were clamped and water cooled at both ends. The center part was heated to the target temperature under the control with a thermocouple, which was connected to the surface of steel samples at the midpoint of length. The width of the anvil was 10 mm.

Table I. Composition of the Steel Used in the Current Study (wt %)

C	Si	Mn	P	T.S	Al_s	T.Ca	T.Mg	T.O	Fe
0.073	0.18	1.48	0.0082	0.0014	0.021	0.0008	0.0003	0.0019	balanced

Three tests as listed in **Table II** were performed in a vacuum of $5x10^{-3}$ mbar. Samples A and B were heated to 1673 K and 1723 K respectively at the rate of 5 K/s. After holding for 2 minutes, the plain strain compression was performed with a 30% reduction, followed by a rapid cooling. Sample C was first heated to 1723 K and held for 2 minutes, then cooled down to 1673 K at the rate of -5 K/s before soaking for another 2 minutes. After that, a 30% reduction was carried out before the rapid cooling. The reduction of 30% was chosen based on pre-experiments, as 30% was the maximum reduction that could be performed without steel leakage when the deformation was carried out on semi-solid steel samples.

Table II. Three Experiments

Sample	Temperature 1 (K)	Holding time 1 (s)	Temperature 2 (K)	Holding time 2 (s)	Reduction (%)	Strain rate (s^{-1})
A	1673	120	-	-	30%	5
B	1723	120	-	-	30%	5
C	1723	120	1673	120	30%	5

Metallographic samples were cut from the center of steel samples after deformation, as shown in **Figure 1**. A FEI Versa 3D was used for the analysis of inclusions, concentrating on the dash area, which was 3 mm in width and about 7 mm along sample thickness. In order to eliminate errors caused by the temperature gradient and the randomness of aspect ratio (the ratio of the maximum to minimum diameter of inclusions) of small inclusions, only >5 μm inclusions in the 3 mm x 3 mm center area were selected to analyze the deformation of inclusions. Inclusions in the metallographic sample cut from the original pipeline steel slab was also analyzed to provide a baseline.

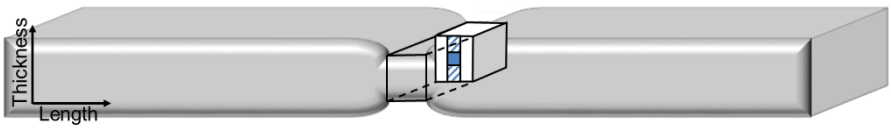

Fig. 1- Sampling of metallographic sample

Stress-strain curves of sample A and sample C during plain strain compression at 1673 K were similar. As shown in Figure 2, the maximum stress of sample A and sample C was 107 MPa and 105 MPa, while that of sample B was only 50 MPa, indicating that the steel sample at 1723 K was softer than the other two samples at 1673 K during deformation. It should be noted that the small fluctuation at the beginning of the stress-strain curve was considered as a tolerable error, which was caused by the equipment. Shrinkage cavities were observed in the center of the steel sample heated to 1723 K without deformation. It indicated that when the surface temperature reached 1723 K, a semi-solid zone was formed in the center part of sample B and sample C as a joint result of direct resistance heating, water cooling at both ends, and heat radiation from the sample surface to the surroundings. While the deformations of sample A and sample C at 1673 K were pure solid.

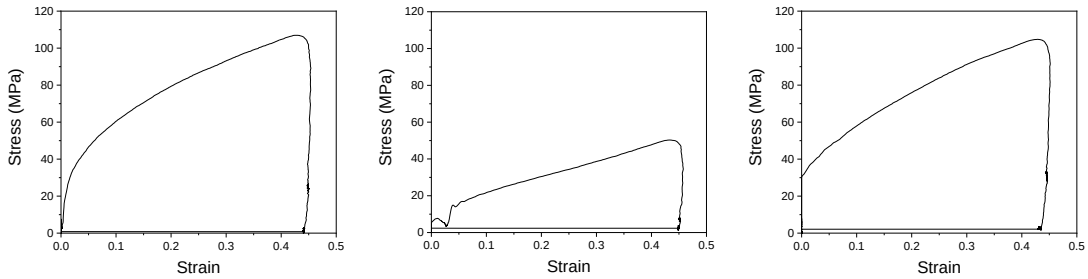

(a) (b) (c)

Fig. 2- Stress-strain curves during deformation
(a) sample A, (b) sample B, and (c) sample C

The average aspect ratio of inclusions in the same layer along sample thickness was plotted in **Figure 3 (a)-(c)**. A parabolic pattern was shown along sample thickness with the highest value in the middle, which was in consistence with the strain distribution of general rolling samples[13, 14]. The average aspect ratio of inclusions in the 3 mm x 3 mm center area of each sample was compared in **Figure 3 (d)**. A small area of 9 mm^2 was chosen so that the analysis area in sample B was limited to the semi-solid zone to maintain the sample characteristics and eliminate the effect of the solid shell. The average aspect ratio of inclusions in the original slab was 1.23. For sample A, after deformed at 1673 K, it increased to 1.29. While for sample B and sample C, they were 1.61 and 1.89, respectively.

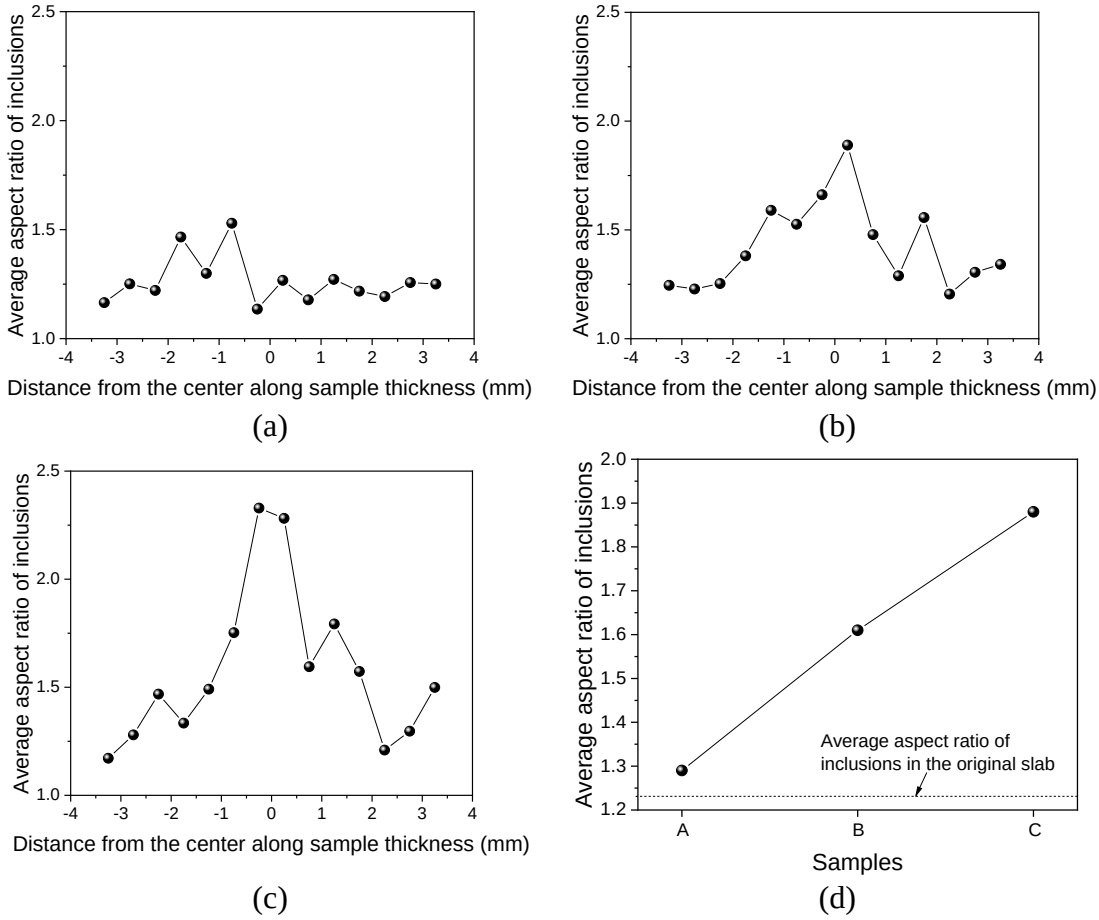

Fig. 3- Average aspect ratio of inclusions in (a) sample A, (b) sample B, (c) sample C, and (d) their comparison

The deformation of inclusions in sample A was very small because the strain in sample A was concentrated on steel phase, which was softer than the inclusion phase when both phases were solid or near solid at 1673 K. For sample B, it was rather particles flowed in a semi-solid pool under pressure than the strain partitioning between the steel phase and the inclusion phase as in pure solid deformation. It was noted that although both the steel phase and the inclusion phase in sample C were in similar states as those in sample A, the aspect ratio of inclusions in sample C, especially in the center, was significantly higher than both sample A and sample B.

The composition of inclusions in each sample was plotted in the CaO-CaS-Al_2O_3-MgO phase diagrams, as shown in **Figure 4**, where each dot represented an inclusion. The aspect ratio of inclusions was indicated by the size of dot. If the CaS content of the inclusion was higher than the MgO content, it was plotted in the triangle of CaO-CaS-Al_2O_3, otherwise it was in the triangle of CaO-Al_2O_3-MgO. The average composition of inclusions in each sample was plotted as a star. The average composition of inclusions in the original slab was 60.4%Al_2O_3-17.5%CaO-10.8%MgO-11.3%CaS. After the samples was undergone different thermal histories and the followed deformation, the average composition of inclusions in samples A to C changed to

62.6%Al_2O_3-11.4%CaO-10.1%MgO-16.0%CaS, 58.0%Al_2O_3-22.8%CaO-14.4%MgO-4.8%CaS, and 59.8%Al_2O_3-14.1%CaO-11.6%MgO-14.3%CaS, respectively. The content of Al_2O_3 and MgO of inclusions in samples A to C was similar. Compared to inclusions in the original slab, the CaS content increased by 4.6% in sample A, which was heated up to 1673 K and soaked for 2 minutes before deformation. While the CaS content decreased by 6.5% in sample B after being heated for 2 minutes under 1723 K. For sample C, the thermal history of which combined those of sample A and sample B, the CaS content of inclusions was closed to, but a little lower than that of sample A. The CaO content of the inclusion in steel samples was sample B > original slab >sample C >sample A, which was opposite to the CaS content. There was no obvious variation trend of the number density of inclusions. More dots were shown in Fig. 4 (a) because the scanning area of inclusions in the original slab was much bigger than the other steel samples. The variation of number density was probably due to the limited number of inclusions selected for deformation analysis.

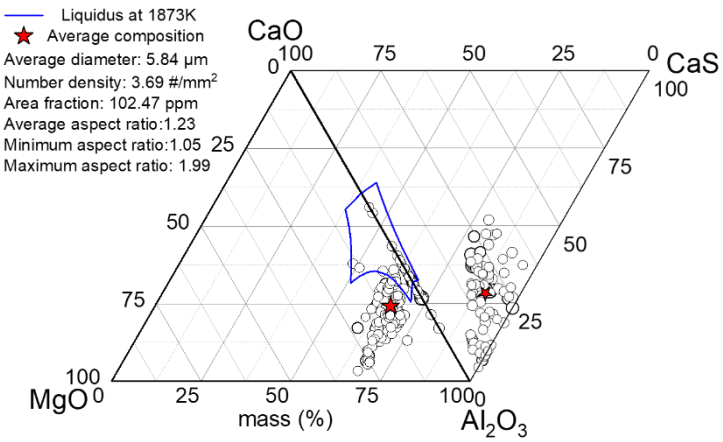

(a)

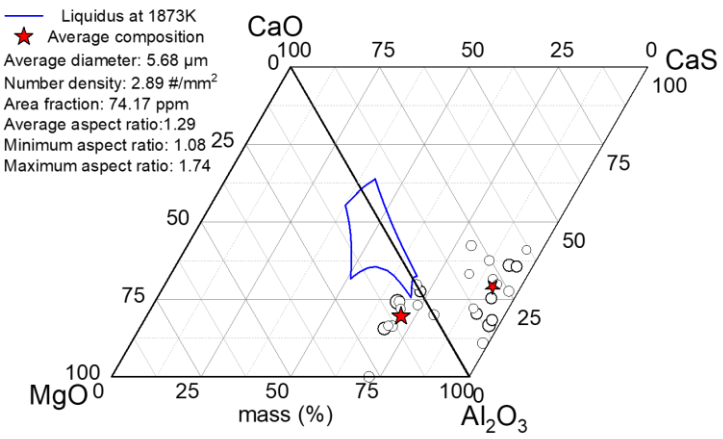

(b)

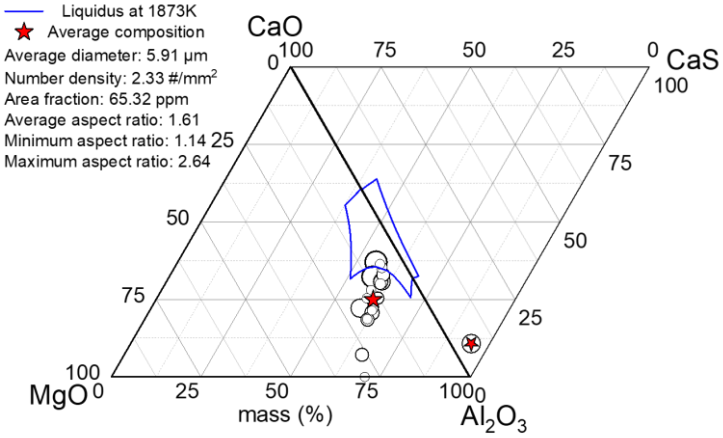

(c)

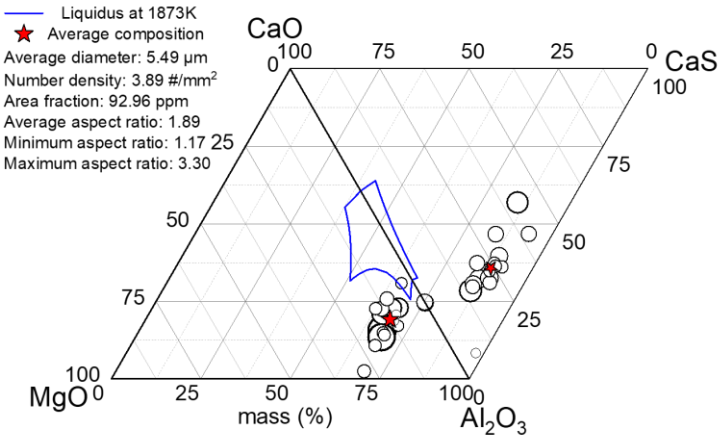

(d)

Fig. 4- Composition of inclusions in (a) original slab, (b) sample A, (c) sample B, and (d) sample C

The elemental mapping of typical inclusions in each sample was shown in **Figure 5**. Inclusions in the original slab were near-spherical Al_2O_3-MgO-CaO with a slight CaS outer layer. After deformation trials, MgO·Al_2O_3 phase, Al_2O_3-CaO-(MgO) phase, and varied amounts of CaS·phase existed in inclusions. The amount of CaS outer layer was consistent with the average composition of inclusions mentioned above. There was a thicker CaS outer layer in sample A and a thinner one in sample B.

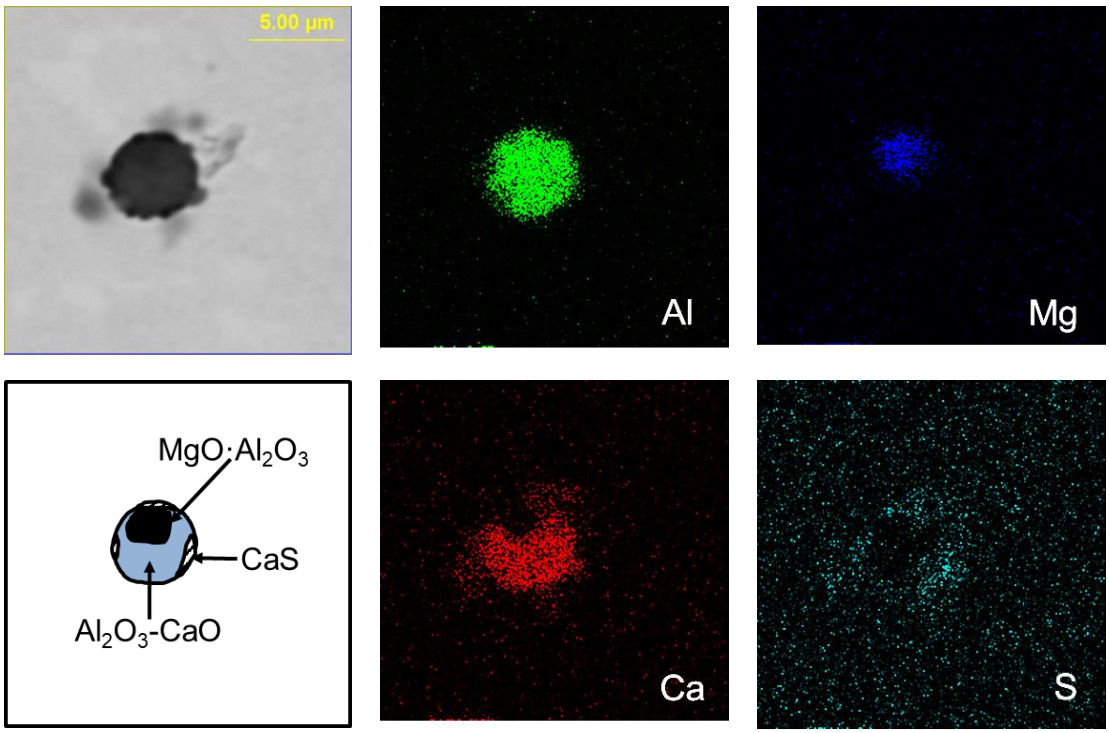
5.00 µm
Al
Mg
MgO·Al2O3
CaS
Al2O3-CaO
Ca
S

(a)

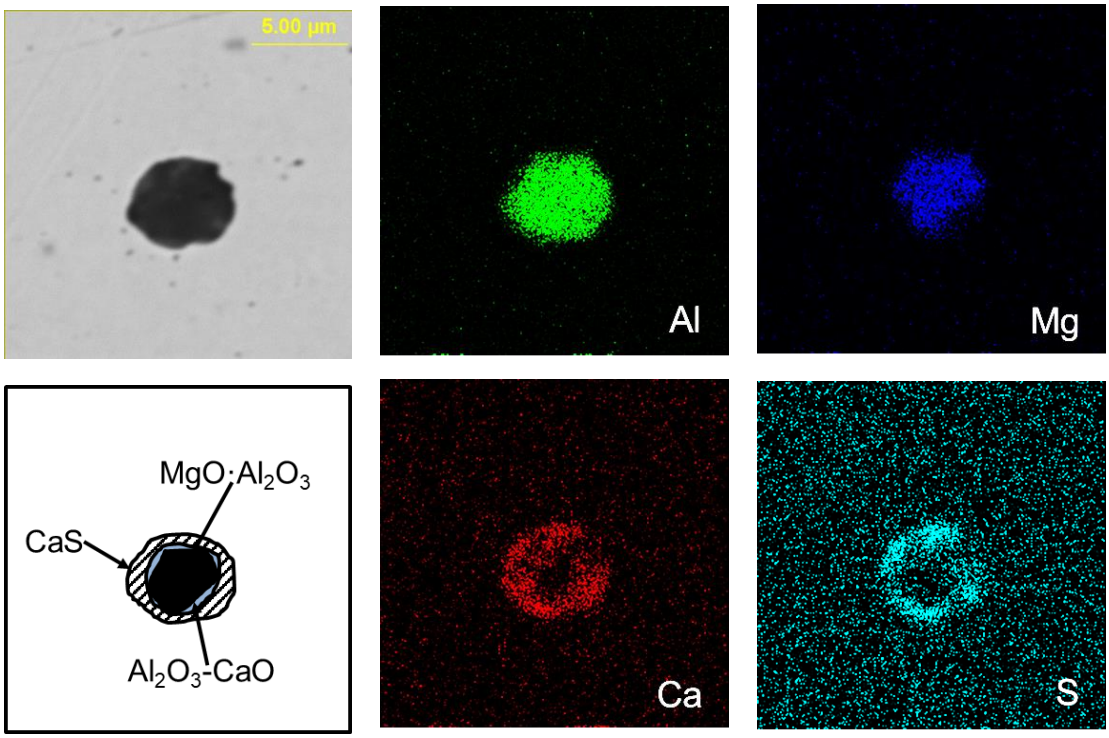
5.00 µm
Al
Mg
MgO·Al2O3
CaS
Al2O3-CaO
Ca
S

(b)

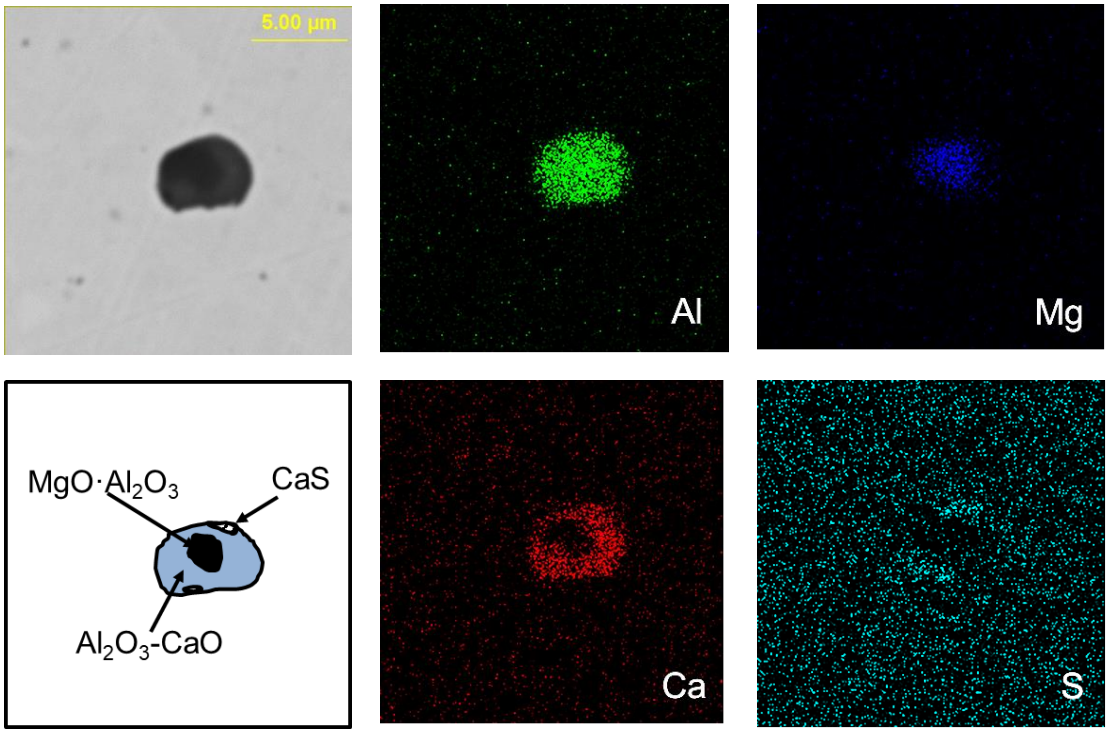

(c)

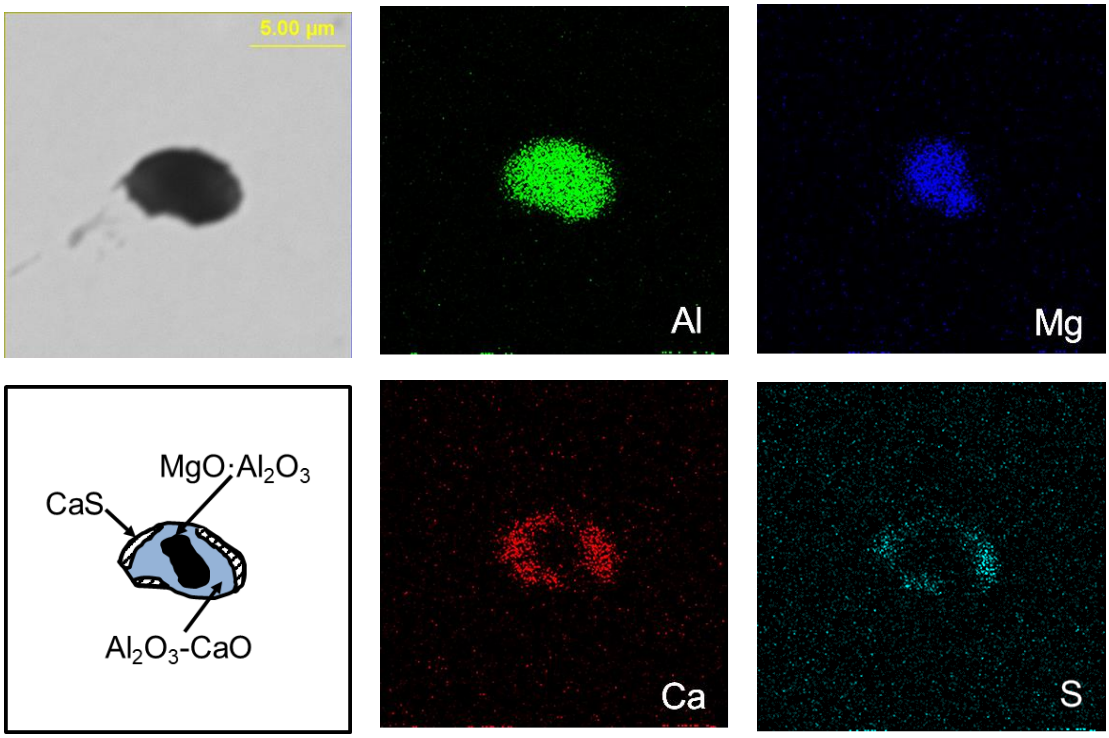

(d)

Fig. 5- Elemental mapping of typical inclusions in (a) original slab, (b) sample A, (c) sample B, and (d) sample C

Thermodynamic calculation for the transformation of inclusions was preformed using the thermodynamic software FactSage 7.0 with databases of FactPS, FToxid, and FSstel[15, 16]. Phases in the inclusions during solidification and cooling process of the

pipeline steel were shown in **Figure 6**. Inclusions were liquid calcium-aluminate and solid spinel in the molten steel. As the temperature decreased during the solidification of the steel, the liquid phase was transformed to solid phases of $CaO{\cdot}2Al_2O_3$, $MgO{\cdot}Al_2O_3$, and CaS at the temperature between liquidus and solidus of the steel. During further cooling process of the steel, $CaO{\cdot}2MgO{\cdot}8Al_2O_3$ phase and CaS phase precipitated, while the amount of $MgO{\cdot}Al_2O_3$ phase decreased. The inclusion was transformed from Al_2O_3-CaO-MgO to Al_2O_3-CaS-MgO-CaO, which agreed with the transformation between CaO and CaS in sample A and sample B. It should be noticed that the temperature in the center of the sample was higher than that detected by the thermocouple that was connected to the surface of the steel sample.

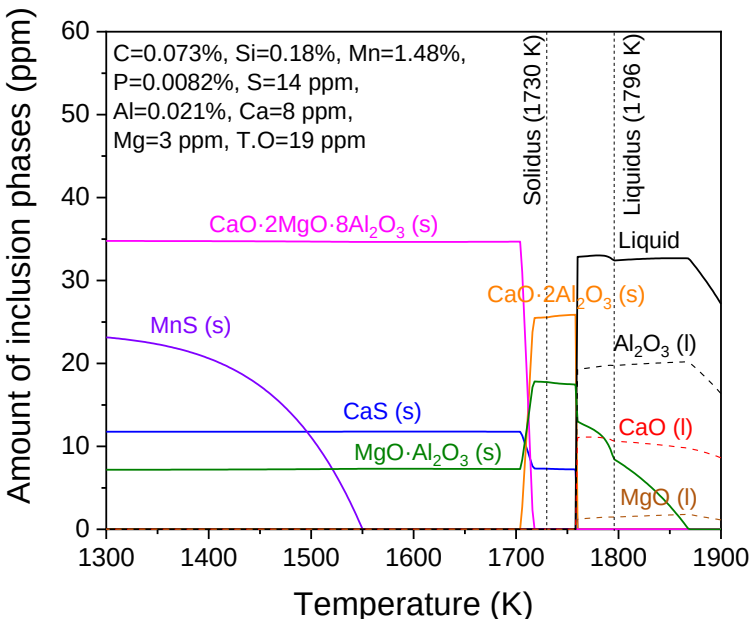

Fig. 6- Transformation of inclusions during solidification and cooling process of the steel

A kinetic model was developed to simulate the dynamic transformation in the composition of inclusions during the cooling and second soaking process of sample C. It was assumed that the inclusion was homogeneous, the transformation rate of the inclusion was controlled by the element diffusion between the steel matrix and the inclusion, and the local equilibrium was achieved at the steel-inclusion interface. The main reaction between the inclusion and the steel matrix is presented by Eq.[1]. Diffusion rate of Al, Mg, Ca, S, and O in the steel is shown by Eq.[2]. Details of the kinetic model was presented elsewhere[17].

$$3x(Al_2O_3)+3y(CaO)+2(y-z)[Al]+3z[Mg]+3y[S]=(3x+y-z)(Al_2O_3)+3z(MgO)+3y(CaS) \quad [1]$$

$$\frac{dm}{dt}=\frac{[\%i]_{\text{bulk}}-[\%i]_{\text{int}}}{100}4\pi Dr\rho_{\text{steel}} \quad [2]$$

Where [%i] is the mass percentage of element; D is the diffusivity, m^2/s; r is the radius

of the inclusion, m; and ρ_{steel} is the density of the steel matrix, kg/m^3. Eq. [1] was given based on the detected inclusion composition and the evolution of inclusion composition from thermodynamic calculation. CaS precipitated at the interface of the inclusion phase and the steel matrix. The element of [S] came from the steel matrix, while [Ca] originated from calcium aluminate. Dissolved [Al] and [Mg] diffused from the steel matrix to the interface, and reacted with calcium aluminate. From the calculation results of FactSage 7.0, the equilibrium mass fractions of [Mg] in the steel matrix were 1.1055x10^{-8} at 1723 K and 6.7224x10^{-9} at 1673 K, which were higher than the [Ca] contents of 9.5055x10^{-12} and 3.1452x10^{-12} at corresponding temperature. Therefore, though the mass fraction of total calcium (T.Ca) in the steel was higher than that of the total magnesium (T. Mg), as shown in Table I, [Mg] was included in Eq. [1] instead of [Ca].

After heating up to 1723 K and holding for 2 minutes as sample B, the temperature of sample C was decreased to 1673 K within 10 s, followed by another 2 minutes of soaking. Taking the detected composition of inclusions in sample B as the basis, the transformation in the composition of inclusions during the cooling and second soaking process of sample C is shown in **Figure 7**. The content of CaO in inclusions decreased, while CaS content increased. The transformation rate of inclusions was relatively high, as 1673 K was a high temperature comparing to the heating treatment temperature commonly used[10].

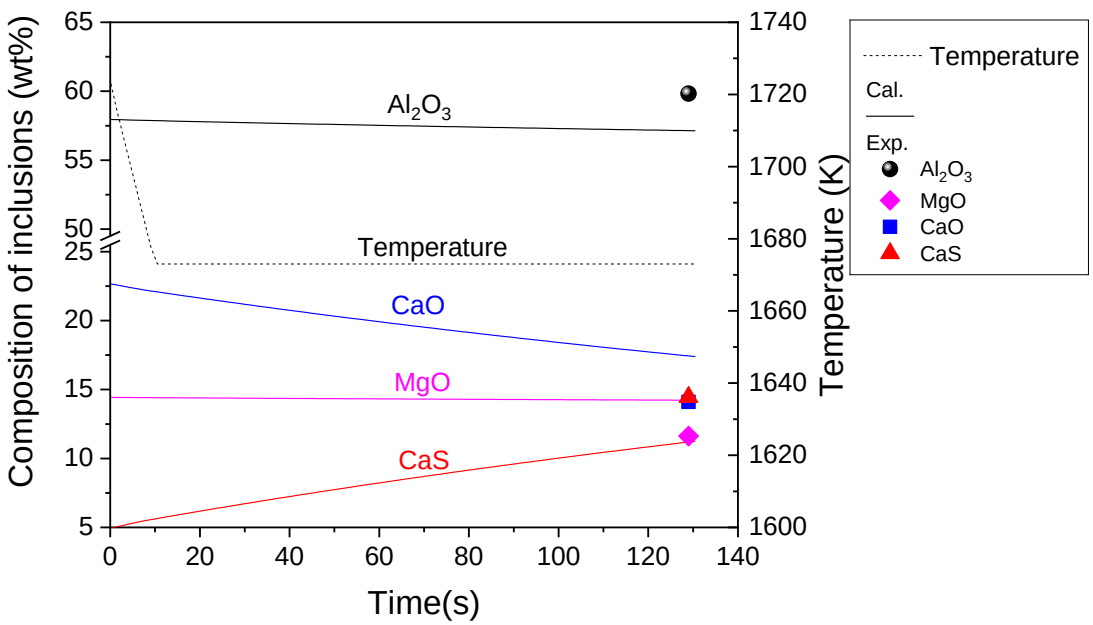

Fig. 7- Kinetic variation of the composition of inclusions with time

The thermodynamic calculation (**Figure 6**) explained the difference between sample A and B, while the kinetic model (**Figure 7**) presented that between sample B and C.

Based on the transformation of inclusions discussed above, the difference in the deformation of inclusions among steel samples undergoing various thermal histories is explained by **Figure 8**. Represented by the shaded area in the lower part of **Figure 8**, the sum strains of the inclusion phase and the steel matrix were equal among samples deformed under the same reduction. The aspect ratio of inclusions after the deformation was dominated by the strain partitioning, which was caused by the difference of the hardness between the inclusion phase and the steel phase[18, 19]. The data of hardness of inclusion phases at high temperature was not available. But generally speaking, the inclusion phase with a higher melting point tended to exhibit a higher hardness[20]. The melting point of CaS was 2673 K, which was much higher than that of calcium-aluminates. Therefore, when steel samples were deformed in the solid state at 1673 K, with a similar $MgO{\cdot}Al_2O_3$ core in the center, inclusions in sample C were softer than those in sample A due to a thinner hard CaS outer layer, while the hardness of the steel matrix was almost the same. More stain concentrated on the soft phase than the hard phase[21]. The total strain of the inclusion phase shown by the dark color in the lower part of **Figure 8** was larger in sample C than that of sample A, resulting in a higher aspect ratio of inclusions after the deformation. For the deformation in the semi-solid steel, although the inclusion phase was softer than those in the other two solid samples, the hardness of the semi-solid steel phase was also much lower. The smaller hardness difference between the soft inclusion phase and the soft steel matrix caused that the aspect ratio of inclusions in sample B was between those in sample A and sample C.

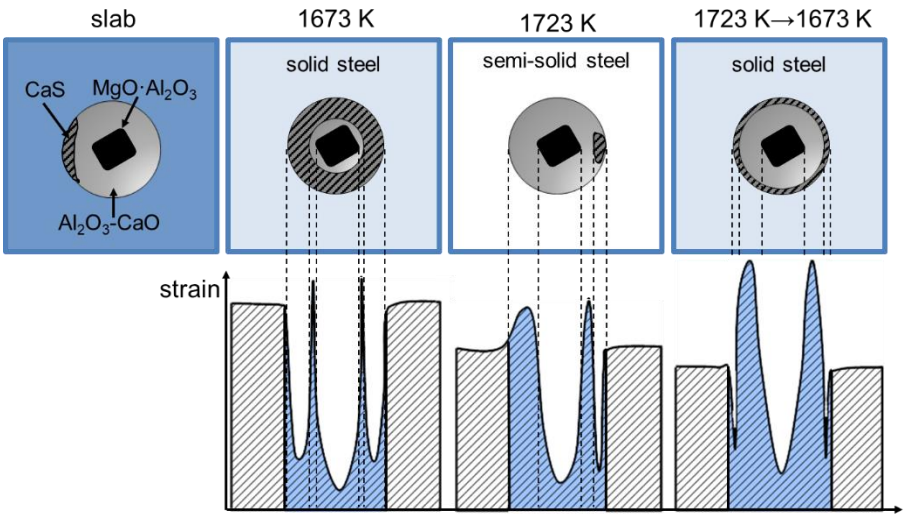

Fig. 8- Schematic deformation mechanism of inclusions in the steel under different thermal history

In conclusion, the deformation of inclusions was influenced by the thermal history of the steel during plain strain compression. Under the same deformation temperature of 1673 K, the aspect ratio of inclusions in the persistent heating sample was significantly lower than that in the sample going through melting and solidification process in the current study. The aspect ratio of inclusions in the steel deformed in

semi-solid state at 1723 K was between those of the former two. The transformation of inclusions in steel samples undergone different thermal histories caused various amounts of CaS precipitated in the outer layer of inclusions. The variation of the inclusion aspect ratio was explained by the strain partitioning caused by the hardness difference between the inclusion phase and the steel phase.

Acknowledgements

The authors are grateful for support from the National Natural Science Foundation of China (Grant No. U1860206, No. 51725402, No. 51874032), the High Steel Center (HSC) at Yanshan University and University of Science and Technology Beijing, and Beijing International Center of Advanced and Intelligent Manufacturing of High Quality Steel Materials (ICSM) at University of Science and Technology Beijing (USTB), China.

References:

[1] C. Devadas, I. V. Samarasekera, and E. B. Hawbolt: Metall. Trans. A, 1991, vol. 22A, pp. 335-49.

[2] M. F. Buchely, D. M. Field, and D. C. Van Aken: Metall. Mate. Trans. B, 2019, vol. 50B, pp. 1180-92.

[3] A. M. El-Wazri, F. Hassani, S. Yue, E. Es-Sadiqi, L. E. Collins, and K. Iqbal: Trans. Iron Steel Inst. Jap., 2007, vol. 39, pp. 253-62.

[4] S. Akhlaghi, and S. Yue: ISIJ Int., 2001, vol. 41, pp. 1350-6.

[5] D. Zhao, H. Li, C. Bao, and J. Yang: ISIJ Int., 2015, vol. 55, pp. 2115-24.

[6] A. Dehghan-Manshadi, and R. Dippenaar: Metall. Mater. Trans. A, 2010, vol. 41A, pp. 3291-6.

[7] R. Maiti, and E. Hawbolt: J. Mater. Energy Syst., 1985, vol. 6, pp. 251-62.

[8] W. Yang, C. Guo, L. Zhang, H. Ling, and C. Li: Metall. Mater. Trans. B, 2017, vol. 48B, pp. 2717-30.

[9] Q. Ren, Y. Zhang, Y. Ren, L. Zhang, J. Wang, and Y. Wang: J. Mater. Sci. Technol.,

2021, vol. 61, pp. 147-58.

[10] Y. Chu, W. Li, Y. Ren, and L. Zhang: Metall. Mater. Trans. B, 2019, vol. 50B, pp. 2047-62.

[11] J. Guo, S. Cheng, and Z. Cheng: ISIJ Int., 2013, vol. 53, pp. 2142-51.

[12] H. Iwai, B. Tsujino, S. Isa, and T. Ao: Tetsu-to-Hagane, 1968, vol. 54, pp. 1037-46.

[13] J. H. Beynon, and C. M. Sellars: J. Test. Eval., 1985, vol. 13, pp. 28-38.

[14] R. Colas, and C. M. Sellars: J. Test. Eval., 1987, vol. 15, pp. 342-9.

[15] C. Bale, P. Chartrand, S. Degterov, G. Eriksson, K. Hack, R. Mahfoud, J. Melançon, A. Pelton, and S. Petersen: Calphad, 2002, vol. 26, pp. 189-228.

[16] S. Nurmi, S. Louhenkilpi, and L. Holappa: Steel Res. Int., 2009, vol. 80, pp. 436-40.

[17] Y. Ren, L. Zhang, and C. Pistorius: Metall. Mater. Trans. B, 2017, vol. 48B, pp. 2281-92.

[18] K. Gove, and J. Charles: Metals Technol., 1974, vol. 1, pp. 425-31.

[19] T. Baker, K. Gave, and J. Charles: Metals Technol., 1976, vol. 3, pp. 183-93.

[20] D. Ladutkin, E. Korte, M. Bleymehl, C. Bruch, and K. Doppler: Bearing Steel Technol., 2017, vol. 11, pp. 48-62.

[21] C. Elango, S. Yu, K. Naoya, M. Goro, and F. Tadashi: Metall. Mater. Trans. A, 2019, vol. 50A, pp. 4111–26.

CAPTIONS:

LIST OF TABLES

Table I. Composition of the Steel Used in the Current Study (wt %)

Table II. Three Experiments

LIST OF FIGURES

Fig. 1- Sampling of metallographic sample

Fig. 2- Stress-strain curves during deformation (a) sample A, (b) sample B, and (c) sample C

Fig. 3- Average aspect ratio of inclusions in (a) sample A, (b) sample B, (c) sample C, and (d) their comparison

Fig. 4- Composition of inclusions in (a) original slab, (b) sample A, (c) sample B, and (d) sample C

Fig. 5- Elemental mapping of typical inclusions in (a) original slab, (b) sample A, (c) sample B, and (d) sample C

Fig. 6- Transformation of inclusions during solidification and cooling process of the steel

Fig. 7- Kinetic variation of the composition of inclusions with time

Fig. 8- Schematic deformation mechanism of inclusions in the steel under different thermal history